Covalent Organic Frameworks

International Edition: DOI: 10.1002/anie.201915569
German Edition: DOI: 10.1002/ange.201915569

A Corrole-Based Covalent Organic Framework Featuring Desymmetrized Topology

Yanming Zhao[+], Wenhao Dai[+], Yunlei Peng, Zheng Niu, Qi Sun, Chuan Shan, Hui Yang, Gaurav Verma, Lukasz Wojtas, Daqiang Yuan, Zhenjie Zhang, Haifeng Dong,* Xueji Zhang,* Bao Zhang,* Yaqing Feng, and Shengqian Ma**

Abstract: *Herein, for the first time, we present the successful synthesis of a novel two-dimensional corrole-based covalent organic framework (COF) by reacting the unusual approximately T-shaped 5,10,15-tris(p-aminophenyl)corrole H_3TPAPC with terephthalaldehyde, which adopts desymmetrized* ***hcb*** *topology and consists of a staggered AB stacking structure with elliptical pores. The resultant corrole-based COF,* ***TPAPC-COF****, exhibits high crystallinity and excellent chemical stability. The combination of extended π-conjugated backbone and interlayer noncovalent π–π interactions endows* ***TPAPC-COF*** *with excellent absorption capability in the entire visible-light and even near-infrared regions. Moreover, this work suggests the promise of* ***TPAPC-COF*** *as a new class of photoactive material for efficient singlet-oxygen generation with potential photodynamic therapy application as demonstrated by in vitro anticancer studies.*

Coinciding with the development of synthetic methodologies for the preparation of free-base corroles, corrole chemistry has witnessed an immense boost in the last two decades, with reports ranging from syntheses to properties to applications.[1] Specially, corroles as the 18π electron tetrapyrrolic macrocycles from the porphyrinoid family, display a unique structure with a direct pyrrole–pyrrole link containing a smaller cavity and three protons in the inner core of the contracted ring, affording attractive, distinctive photophysical properties and coordination chemistry as well as a specific chemical reactivity.[2] Owing to these prominent features,this burgeoning class of macrocyclic compounds shows great potential in diverse fields including catalysis,[3] energy conversion,[4] chemical sensors,[5] optoelectronics,[2b,6] and biological/medical applications.[7,8] Due to the versatility of corrole derivatives, it is a bright prospect to explore their functional materials via heterogenization into porous organic polymers (POPs),[4c,9] covalent organic frameworks (COFs),[10] and metal–organic frameworks (MOFs).[11] However, studies that directly introduce these attractive motifs into porous crystalline framework materials for achieving further functionalizations have been barely reported.[11b] Indeed, fine-tuning and controllable construction of networks incorporating corrole moieties remains a great synthetic challenge. Herein, we report for the first time the successful construction of a corrole-based COF from a C_{2v}-symmetric tridentate corrolic unit.

Covalently constructed by a bottom-up approach from molecule building blocks, COFs are an emerging class of crystalline, porous, extended polymers with highly ordered and periodic two-dimensional (2D) or three-dimensional (3D) framework structures and have received tremendous attention in various applications.[12] Important characteristics of COFs for which they are renowned include their high surface area and permanent porosity, their precise design and control over both skeletons and pores, and their fine-tuned chemical and physical properties.[13] Nonetheless, from the viewpoint of the structural diversity, the field of COFs is still in its early stage especially when compared with the impressive success of MOFs,[11,12e] thereby confining their application scope. Direct introduction of new building blocks for constructing novel COFs has been considered as one of the most straightforward approaches in augmenting the

[*] Y. Zhao,[+] Prof. B. Zhang, Prof. Y. Feng
School of Chemical Engineering and Technology, Tianjin University
Tianjin 300350 (China)
E-mail: baozhang@tju.edu.cn

Y. Zhao,[+] Dr. Z. Niu, Dr. Q. Sun, C. Shan, Dr. H. Yang, G. Verma, Dr. L. Wojtas, Prof. S. Ma
Department of Chemistry, University of South Florida
4202 East Fowler Avenue, Tampa, FL 33620 (USA)
E-mail: sqma@usf.edu

W. Dai,[+] Prof. H. Dong
Research Center for Bioengineering and Sensing Technology
University of Science & Technology Beijing
Beijing 100083 (China)
E-mail: hfdong@ustb.edu.cn

Y. Peng, Prof. Z. Zhang
College of Chemistry, Nankai University
Tianjin 300071 (China)
E-mail: zhangzhenjie@nankai.edu.cn

Prof. D. Yuan
State Key Laboratory of Structure Chemistry
Fujian Institute of Research on the Structure of Matter
Chinese Academy of Sciences, Fuzhou 350002 (China)

Y. Zhao,[+] Prof. Y. Feng
Collaborative Innovation Center of Chemical Science and Engineering, Tianjin 300072 (China)

Prof. X. Zhang
School of Biomedical Engineering
Shenzhen University Health Science Center
Shenzhen, Guangdong 518060 (China)
E-mail: zhangxueji@szu.edu.cn

[+] These authors contributed equally to this work.

Supporting information and the ORCID identification number for one of the authors of this article can be found under: https://doi.org/10.1002/anie.201915569.

diversity of COF structures. Moreover, it is worth noting that the size, symmetry, and connectivity of the linkers in general determine the geometry of the resulting framework, in which structural desymmetrization represents an available yet effective avenue to achieve more intriguing architectures,[12e,14] in contrast to most reported cases in which the principle of high-symmetry-guided design is expected to generate desirable networks (Table S3). Several different strategies for the formation of desymmetric COFs have been reported,[14] including changing angles between points of extension without altering connectivity,[15a] changing extension lengths within an individual linker,[15b] shape-persistent-patch design,[15c] and the mixed-component approach.[15d] Nevertheless, constructing such a COF based on the angle-specific vertex design is difficult due to the challenges on structural synthesis and control, which has been rarely achieved.[15a]

Bearing the above in mind, we attempted to construct a corrole-based COF for both its importance in realizing the functionality of corrole-based porous materials and its great potential in enriching the COF network structures, given the unusual approximately T-shaped geometry of the corrole monomer and its exploration vacancy in the synthesis of COF materials.

With a view to optoelectronic properties, 2D COFs are of particular interest due to the favorable electron delocalization on the polymeric backbone, with extended π-conjugations and layer stacking architectures forming periodic columnar π-arrays with significant electronic overlap.[16] In this context, with the incorporation of certain photoelectric components into well-defined 2D COFs, the resultant materials can possess unique features such as photoactivation of molecular oxygen,[17] photoconductivity,[18] white light emission,[19] charge-carrier transport,[20] and ionic conductivity.[21] Considering the interesting photoactive properties of corrole derivatives and their promising biological applications, we envision that incorporation of corrole moieties into 2D COF would allow for the observation of distinctive optical performance and the potential in tailoring to a specific application.

In this study, we report the targeted synthesis of the first 2D corrole-based COF with a desymmetrized structure, assigned as **TPAPC-COF**, starting from the approximately T-shaped, C_{2v}-symmetric 5,10,15-tris(*p*-aminophenyl)corrole H_3TPAPC and liner terephthalaldehyde (TA) connected through the [3+2] imine condensation reaction, which exhibits excellent chemical stability and has a Brunauer—Emmett–Teller (BET) surface area of 745 $m^2 g^{-1}$. Our studies show that **TPAPC-COF** adopts an unusual dissymmetric **hcb** topology and consists of a staggered AB stacking structure with elliptical pores. As expected, the extended π-conjugated system endows **TPAPC-COF** with enhanced light-harvesting capability in the long-wavelength visible and NIR regions. Furthermore, we demonstrate that **TPAPC-COF** can serve as a photoactive material promoting efficient singlet oxygen ($^1O_2$) generation. The results of anticancer studies in vitro indicate that **TPAPC-COF** has potential for photodynamic therapy (PDT).

Heating a mixture of H_3TPAPC and TA (2:3) in *n*-butanol/mesitylene/acetic acid (10:5:1, by vol.) at 120 °C for 72 h gave the highly crystalline **TPAPC-COF** as a dark powder in 86 % yield (Scheme 1). The resultant **TPAPC-COF** displayed excellent chemical stability after immersion in common organic solvents and aqueous solutions over pH range of 3 to 12 for 72 h, as evidenced by the intact powder X-ray diffraction (PXRD) patterns (Figure S4). The Fourier transform infrared (FTIR) spectra of **TPAPC-COF** showed the typical stretching vibration band of the imine group at

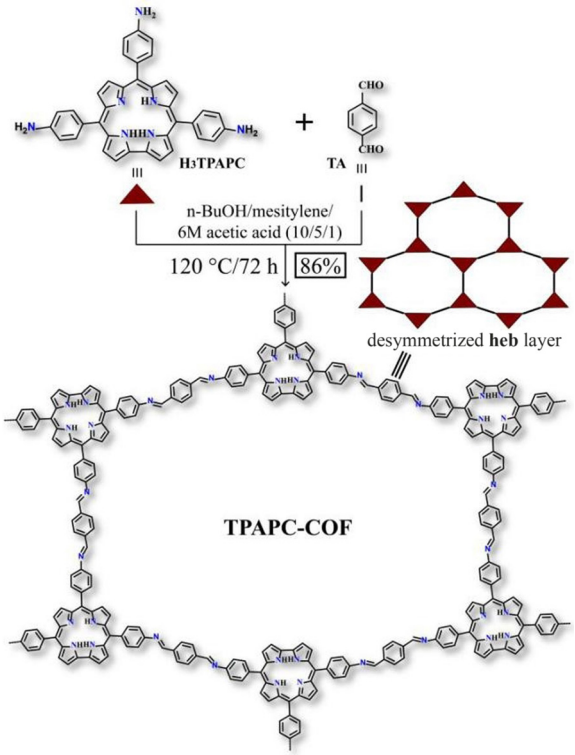

Scheme 1. Schematic representation of the synthesis of **TPAPC-COF**.

1620 cm^{-1}, indicative of its successful polymerization (Figure S5). From the ^{13}C cross-polarization magic-angle-spinning (CP-MAS) NMR spectrum, the characteristic resonance signal of carbon at 156.4 ppm for **TPAPC-COF** further confirmed the establishment of imine bond (Figure S7). Thermogravimetric analysis (TGA) showed that **TPAPC-COF** is stable up to 400 °C under nitrogen atmosphere (Figure S8).

In order to elucidate the structure and unit cell parameters of **TPAPC-COF**, PXRD measurements in conjugation with simulations were carried out. Since **TPAPC-COF** was constructed with the unusual C_{2v}-symmetric tridentate building block H_3TPAPC and the linear building block TA, we assumed that such a combination should yield a lattice with **hcb** topology, as confirmed by calculated results. Obviously in contrast to those COFs reported with an **hcb** net that exhibit hexagonal pores,[14] **TPAPC-COF** affords a dissymmetric structure with elliptical pores (Figure 1 b). As displayed in Figure 1 a, the experimental PXRD pattern shows four intense peaks at $2\theta = 3.35°$, 3.86°, 6.15°, and 7.02° for **TPAPC-COF**, along with other minor peaks, indicating

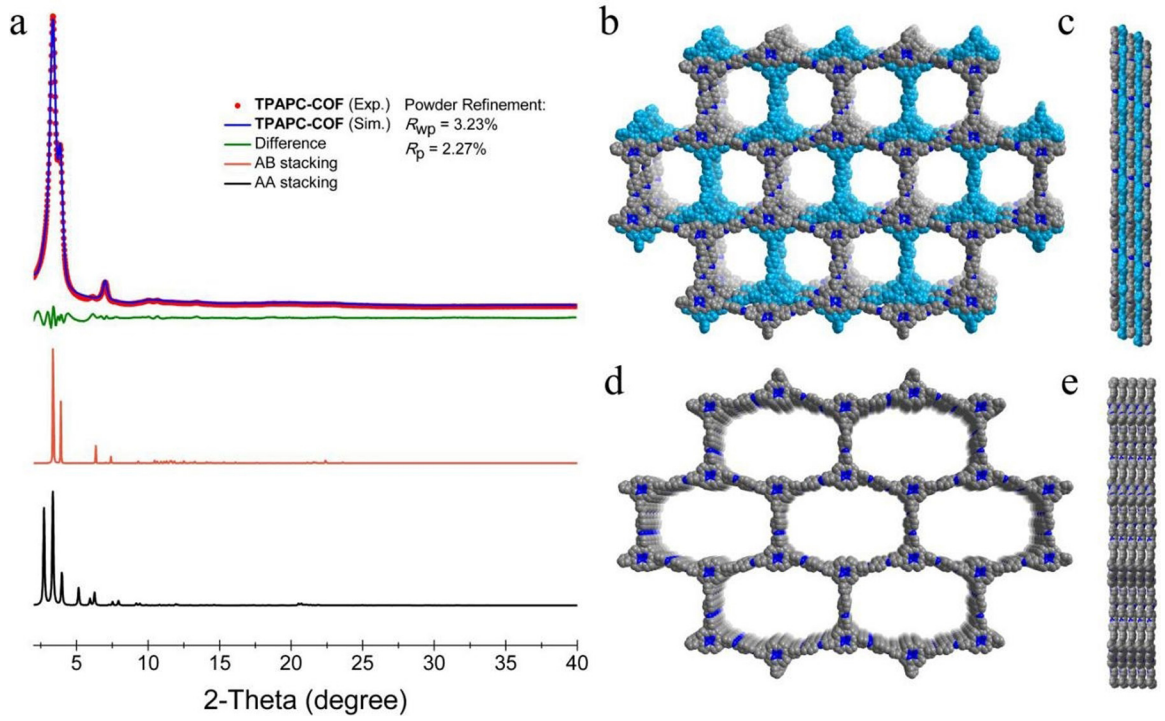

Figure 1. a) PXRD patterns of **TPAPC-COF** with the experimental in red, Pawley refined in blue, difference between experimental and refined data in olive, and simulated AB and AA stacking in orange and black, respectively. b–e) Space-filling models of **TPAPC-COF**: AB stacking from top (b) and side views (c), AA stacking from top (d) and side views (e).

long-range order in the framework. The possible extended structures were generated by the Materials Studio suite of programs. The structural simulations suggested that **TPAPC-COF** favors the staggered AB stacking model (Figure 1 b,c). In this model, the Pawley refined profile matched well with the experimentally observed pattern, resulting in a good agreement factor ($R_{wp} = 3.23\,\%$ and $R_p = 2.27\,\%$) and a reasonable profile difference (Figure 1 a). The refinement yields unit cell parameters of $a = 52.2892$ Å, $b = 40.7693$ Å, $c = 8.8687$ Å, $\alpha = 95.604°$, $\beta = 104.523°$, and $\gamma = 129.098°$. We also simulated the AA eclipsed configuration for **TPAPC-COF**, in which the calculated PXRD pattern mismatched the observed one (Figure 1 a,d,e). The morphology of the activated **TPAPC-COF** samples was examined by scanning electron microscopy (SEM), which showed the aggregation of granular crystallites affording a sphere-like morphology (Figure 2 a). High-resolution transmission electron microscopy (HRTEM) images revealed the clear crystal lattice of **TPAPC-COF**, which is reasonable for π–π stacking (Figure 2 b). The lattice fringe spacing of 0.31 nm can be measured from the HRTEM image, and is close to the interlayer of **TPAPC-COF**.

The permanent porosity of **TPAPC-COF** was investigated by measuring N_2 sorption isotherms at 77 K on freshly activated samples. Through screening different reaction solvent systems and ratios, the highest BET surface area of **TPAPC-COF** was obtained by using the mixed solvents of *n*-butanol/mesitylene/acetic acid (10:5:1, by vol.) (Table S2 and Figures S2 and S3). As displayed in Figure 2 c, **TPAPC-COF** exhibited the typical type I isotherm with a sharp uptake at a low relative pressure ($P/P_0 < 0.1$), which is a significant feature of microporous materials. The BET model was applied to the isotherm of **TPAPC-COF** for P/P_0 between 10^{-4} and 0.1 to afford a BET surface area of 745 $m^2 g^{-1}$, and the corresponding total pore volume calculated at $P/P_0 = 0.95$ is 0.44 $cm^3 g^{-1}$. Nonlocal density functional theory (NLDFT)

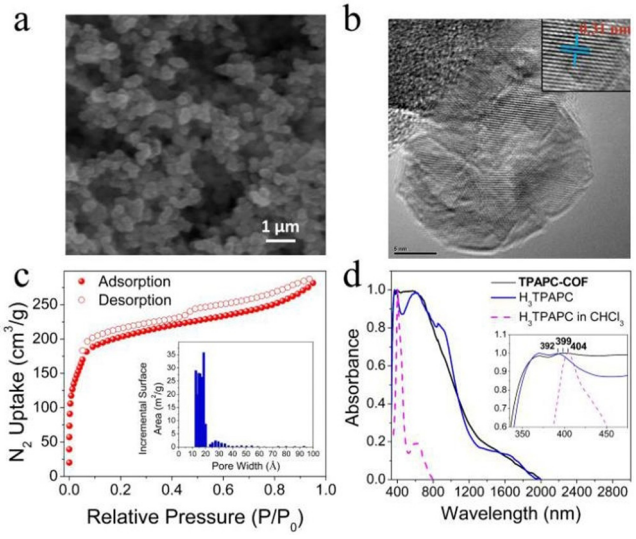

Figure 2. a) SEM image of **TPAPC-COF**. b) HRTEM images of **TPAPC-COF**; the inset shows the lattice distance. c) N_2 sorption isotherms of **TPAPC-COF** at 77 K; the inset shows the pore size distribution. d) Optical absorption spectra of **TPAPC-COF** and the monomer H_3TPAPC measured in diffuse reflectance and H_3TPAPC measured in dilute $CHCl_3$ solution; the inset shows the enlarged region from $\lambda = 335$ to 475 nm.

fitting of the adsorption branch for **TPAPC-COF** provides the pore size distribution with an average pore width of 18.8 Å, close to its simulated value of 23.8 Å (excluding van der Waals radii).

To assess the light-absorption properties of the newly synthesized **TPAPC-COF**, the UV/Vis/NIR absorption spectra were measured. **TPAPC-COF** shows a broad optical response covering the UV and entire visible spectral range, tailing far into the NIR region with an extended absorption to 2000 nm (Figure 2d). It can be seen that **TPAPC-COF** exhibits an absorption band at 399 nm that is due to the Soret band, which is red-shifted by over 7 nm relative to that of the solid H_3TPAPC monomer. Particularly, compared to the observed Q-band peaks in the spectra of the solid corrole monomer and its highly dilute solutions, the spectrum of **TPAPC-COF** displays a continuous absorption without a clear boundary between the Soret and Q-bands. These results indicate its more extensive π-electron delocalization.[22] Meanwhile, for **TPAPC-COF**, the red-shifting of the Soret and Q-bands relative to those of the precursor solution generally demonstrates the increased conjugation extent and π–π stacking-induced charge transfer in the framework.[22c] At longer wavelengths the spectra of **TPAPC-COF** and the solid corrole monomer are nearly identical, indicating similar packing schemes in the COF and solid-state building block.[22a] The optical band gap, based on the absorption onset, is estimated to be 1.06 eV for **TPAPC-COF** (Figure S13).[23] With this small band gap, **TPAPC-COF** is an excellent photoactive material, which can efficiently harvest the sunlight energy and even utilize low-energy photons to generate photoexcited states.

The development of methodologies for efficiently producing $^1O_2$ is of great interest because of its potential application in PDT. One straightforward approach is through the photosensitization between a photosensitizer and molecular oxygen upon irradiation,[24] in which photoactive molecules can be promoted to excited states and undergo intersystem crossing to generate triplet excited states that transfer energy to molecular oxygen for producing $^1O_2$. Encouraged by the strong visible-light absorption of **TPAPC-COF** as well as the capability of obtaining triplet excited states pertaining to corrole molecules (Figure 3a,b),[2b] we employed it for the generation of $^1O_2$.

The photogenerating $^1O_2$ ability of **TPAPC-COF** under 635 nm laser (0.18 W cm^{-2}) irradiation was investigated by using 1,3-diphenylisobenzofuran (DPBF) as a scavenger, and the process was monitored by time-dependent electronic absorption spectroscopy.[22e] As displayed in Figure 3c, irradiation of *N*-methylpyrrolidone (NMP) solutions (1.0 mL) containing DPBF (10 μM) and **TPAPC-COF** (50 μg) led to the steady generation of $^1O_2$, as evidenced by the spectral change of DPBF at $\lambda = 415$ nm. It can be clearly observed from Figure 3d that **TPAPC-COF** exhibited the strong ability to activate molecular oxygen with 90% degradation efficiency of DPBF, whereas monomeric H_3TPAPC showed sharply decreased activity for degrading DPBF with a low conversion of 56%, which indicates that the monomeric system is much less active than **TPAPC-COF**. The activity gap between **TPAPC-COF** and its monomer can be ascribed to

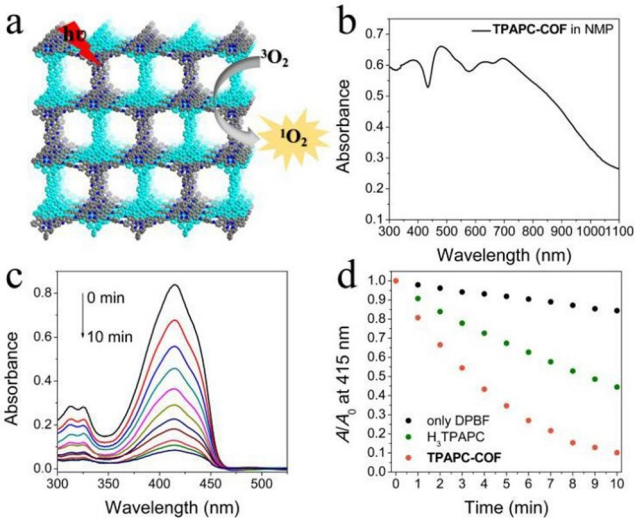

Figure 3. a) Schematic diagram of **TPAPC-COF** generating singlet oxygen. b) Absorption spectrum of **TPAPC-COF** dispersed in *N*-methylpyrrolidone (50 μg mL^{-1}). c) UV/Vis spectra of DPBF solution with **TPAPC-COF** under 635 nm laser (0.18 W cm^{-2}) irradiation for 10 min. d) Quantification of the $^1O_2$ generation ability of DPBF blank, H_3TPAPC, and **TPAPC-COF**.

the facilitated intersystem crossing (responsible for $^1O_2$ generation) of **TPAPC-COF** presumably resulting from its extended π-conjugation and layered stacking architecture with the formation of periodic columnar π-arrays.[25a] Consistent with this, **TPAPC-COF** exhibited weaker fluorescence intensity (Figure S18), with a shorter fluorescence lifetime of 0.082 ns compared with H_3TPAPC (0.19 ns), as determined by time-resolved photoluminescence measurements (Figure S19). The good photoactivity toward producing $^1O_2$ implies that **TPAPC-COF** could serve as a promising photosensitizer for PDT.

The anticancer effect of **TPAPC-COF** was evaluated in vitro. In order to improve its hydrophilicity in the physiological environment, **TPAPC-COF** was firstly modified with an amphiphilic molecule, DSPE-PEG2000, and the resultant composite material afforded a core–shell structure that remained intact and porous (Figure S21–S25), which was assigned as **TPAPC-COF′**. The cytotoxicity of **TPAPC-COF′** was determined by 3-(4,5-dimethylthiazol-2-yl)-2,5-diphenyl-2*H*-tetrazolium bromide (MTT) assay using both normal human dermal fibroblast (NHDF) cells and MCF-7 human breast carcinoma cells. As shown in Figure 4a, **TPAPC-COF′** exhibited no obvious toxicity for NHDF and MCF-7 cells in the dark even at a concentration of 200 μg mL^{-1}, indicating its good biocompatibility. Furthermore, the intracellular $^1O_2$ generation in MCF-7 cells was confirmed by using Singlet Oxygen Sensor Green (SOSG) as an indicator under confocal laser scanning microscopy (CLSM). After MCF-7 cells were incubated with **TPAPC-COF′** at a concentration of 50 μg mL^{-1} and loaded with SOSG, they were irradiated with a 635 nm laser for 5 min, immediately followed by CLSM imaging. **TPAPC-COF′**-treated cells upon irradiation showed strong green fluorescence, whereas a negligible fluorescent signal was detected in all the comparison groups, suggesting

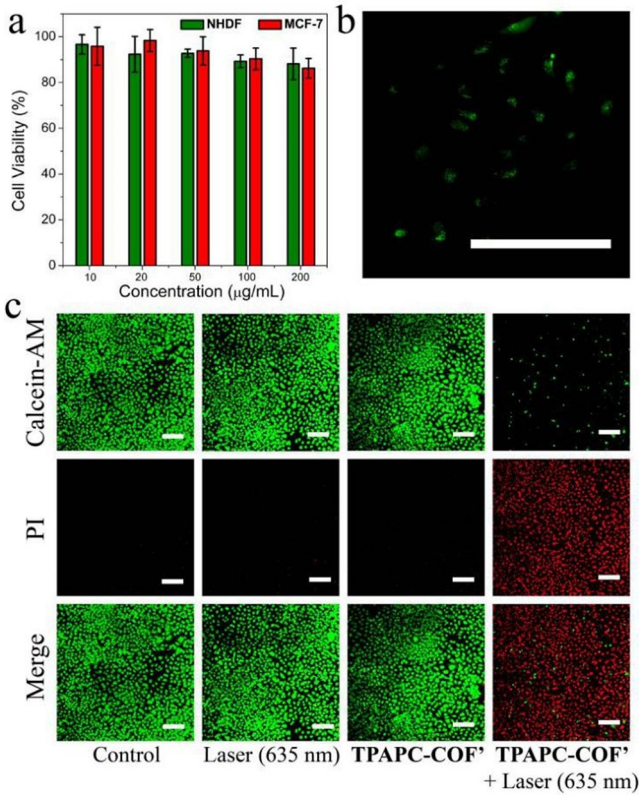

Figure 4. a) The viability of NHDF and MCF-7 cells treated with different concentrations of **TPAPC-COF′** (10, 20, 50, 100, and 200 μg mL^{-1}). b) CLSM of $^1O_2$ generation in MCF-7 cells treated with **TPAPC-COF′** upon irradiation at 635 nm for 5 min. c) CLSM of MCF-7 cells after different treatments: Control, laser (635 nm), **TPAPC-COF′**, and **TPAPC-COF′** + laser (635 nm). All of the scale bars are 200 μm.

that **TPAPC-COF′** is capable of efficiently producing $^1O_2$ in MCF-7 cells (Figure 4b and Figure S26). Finally, we carried out anticancer efficacy experiments to further verify the potential of **TPAPC-COF′** in PDT applications. Compared to the experiments with different treatments, blank, with laser irradiation, or with **TPAPC-COF′** alone, the activity of MCF-7 cells treated with **TPAPC-COF′** upon 635 nm laser irradiation for 10 min is sharply decreased (Figure 4c), and less than 15% of the cancer cells survived (Figure S27b), indicating the remarkable anticancer activity of **TPAPC-COF′**. In contrast, the corrole precursor modified with DSPE-PEG2000 displayed much poorer efficacy in killing cancer cells (Figure S28). It should be pointed out that the structural advantages of corrole-based COF materials clearly contribute to the significant difference in the PDT effect of the modified monomer and **TPAPC-COF′**. Specifically, the nanotechnology platforms used to create the COF nanomaterials can greatly overcome solubility issues, the well-defined ordered COF structure can help control the photoinduced excited states, the well-isolated corrole molecules in the framework can avoid the self-quenching of excited states, and the porous structure can provide a pathway for the facile diffusion of singlet oxygen.[17a,22e,25] These results demonstrate that corrole-COF can serve as an excellent photosensitizer material holding promise for cancer therapy.

In summary, we have reported for the first time the targeted construction of a novel 2D corrole-based COF from the custom-designed H_3TPAPC monomer and TA via imine condensation reaction. The resultant **TPAPC-COF** is highly crystalline with excellent chemical stability and permanent porosity. Interestingly, the geometric uniqueness of the corrole monomer renders **TPAPC-COF** rare desymmetrized **hcb** topology and a staggered AB stacking arrangement with unusual elliptical pores. Our work represents a successful attempt to explore new building blocks for constructing 2D crystalline COF with excellent photoactive properties. **TPAPC-COF** features the a prominently broad spectral response ranging from the UV to NIR regions. Our studies demonstrate that **TPAPC-COF** can serve as an efficient photosensitizer for the generation of singlet oxygen for use in killing cancer cells in vitro. We anticipate that our contribution will not only spur interest in the construction of dissymmetric COFs, but also enrich the applications of corrole-functionalized materials.

Acknowledgements

We acknowledge the China International Science and Technology Project (NO. 2016YFE0114900), National Natural Science Foundation of China (NO. 21761132007), China Scholarship Council (CSC) (NO. 201706250095), United States National Science Foundation (DMR-1352065), and the University of South Florida for financial support of this work.

Conflict of interest

The authors declare no conflict of interest.

Keywords: corrole · covalent organic framework · desymmetrized topology · singlet oxygen

How to cite: *Angew. Chem. Int. Ed.* **2020**, *59*, 4354–4359
Angew. Chem. **2020**, *132*, 4384–4389

[1] a) B. Koszarna, D. T. Gryko, *J. Org. Chem.* **2006**, *71*, 3707–3717; b) A. Ghosh, *Chem. Rev.* **2017**, *117*, 3798–3881; c) Y. Fang, Z. Ou, K. M. Kadish, *Chem. Rev.* **2017**, *117*, 3377–3419; d) J. F. B. Barata, M. G. P. M. S. Neves, M. A. F. Faustino, A. C. Tomé, J. A. S. Cavaleiro, *Chem. Rev.* **2017**, *117*, 3192–3253; e) I. Aviva, Z. Gross, *Chem. Commun.* **2007**, 1987–1999; f) S. Nardis, F. Mandoj, M. Stefanelli, R. Paolesse, *Coord. Chem. Rev.* **2019**, *388*, 360–405.

[2] a) K. E. Thomas, A. B. Alemayehu, J. Conradie, C. M. Beavers, A. Ghosh, *Acc. Chem. Res.* **2012**, *45*, 1203–1214; b) A. Mahammed, Z. Gross, *Coord. Chem. Rev.* **2019**, *379*, 121–132; c) I. Aviv-Harel, Z. Gross, *Coord. Chem. Rev.* **2011**, *255*, 717–736; d) A. Haber, Z. Gross, *Chem. Commun.* **2015**, *51*, 5812–5827; e) R. D. Teo, J. Y. Hwang, J. Termini, Z. Gross, H. B. Gray, *Chem. Rev.* **2017**, *117*, 2711–2729; f) A. Mahammed, Z. Gross, *J. Am. Chem. Soc.* **2005**, *127*, 2883–2887; g) M. Guo, Y.-M. Lee, R. Gupta, M. S. Seo, T. Ohta, H.-H. Wang, H.-Y. Liu, S. N. Dhuri, R. Sarangi, S. Fukuzumi, W. Nam, *J. Am. Chem. Soc.* **2017**, *139*, 15858–15867.

[3] a) A. Mahammed, H. B. Gray, A. E. Meier-Callahan, Z. Gross, *J. Am. Chem. Soc.* **2003**, *125*, 1162 – 1163; b) A. Haber, A. Mahammed, B. Fuhrman, N. Volkova, R. Coleman, T. Hayek, M. Aviram, Z. Gross, *Angew. Chem. Int. Ed.* **2008**, *47*, 7896 – 7900; *Angew. Chem.* **2008**, *120*, 8014 – 8018; c) A. Mahammed, Z. Gross, *Chem. Commun.* **2010**, *46*, 7040 – 7042.

[4] a) D. K. Dogutan, R. McGuire, D. G. Nocera, *J. Am. Chem. Soc.* **2011**, *133*, 9178 – 9180; b) N. Levy, A. Mahammed, M. Kosa, D. T. Major, Z. Gross, L. Elbaz, *Angew. Chem. Int. Ed.* **2015**, *54*, 14080 – 14084; *Angew. Chem.* **2015**, *127*, 14286 – 14290; c) A. Friedman, L. Landau, S. Gonen, Z. Gross, L. Elbaz, *ACS Catal.* **2018**, *8*, 5024 – 5031; d) W. Zhang, W. Lai, R. Cao, *Chem. Rev.* **2017**, *117*, 3717 – 3797.

[5] R. Paolesse, S. Nardis, D. Monti, M. Stefanelli, C. D. Natale, *Chem. Rev.* **2017**, *117*, 2517 – 2583.

[6] L. Flamigni, D. T. Gryko, *Chem. Soc. Rev.* **2009**, *38*, 1635 – 1646.

[7] H. Agadjanian, J. Ma, A. Rentsendorj, V. Valluripalli, J. Y. Hwang, A. Mahammed, D. L. Farkas, H. B. Gray, Z. Gross, L. K. Medina-Kauwe, *Proc. Natl. Acad. Sci. USA* **2009**, *106*, 6105 – 6110.

[8] M. Pribisko, J. Palmer, R. H. Grubbs, H. B. Gray, J. Termini, P. Lim, *Proc. Natl. Acad. Sci. USA* **2016**, *113*, E2258 – E2266.

[9] a) J. Wu, F. Xu, S. Li, P. Ma, X. Zhang, Q. Liu, R. Fu, D. Wu, *Adv. Mater.* **2019**, *31*, 1802922; b) S. Brandès, V. Quesneau, O. Fonquernie, N. Desbois, V. Blondeau-Patissierb, C. P. Gros, *Dalton Trans.* **2019**, *48*, 11651 – 11662.

[10] C. S. Diercks, O. M. Yaghi, *Science* **2017**, *355*, 923 – 930.

[11] a) H. Furukawa, K. E. Cordova, M. O'Keeffe, O. M. Yaghi, *Science* **2013**, *341*, 1230444; b) Y. Zhao, S. Qi, Z. Niu, Y. Peng, C. Shan, G. Verma, L. Wojtas, Z. Zhang, B. Zhang, Y. Feng, Y.-S. Chen, S. Ma, *J. Am. Chem. Soc.* **2019**, *141*, 14443 – 14450.

[12] a) A. P. Côté, A. I. Benin, N. W. Ockwig, M. O'Keeffe, A. J. Matzger, O. M. Yaghi, *Science* **2005**, *310*, 1166 – 1170; b) N. Huang, P. Wang, D. Jiang, *Nat. Rev. Mater.* **2016**, *1*, 16068; c) S. Das, P. Heasman, T. Ben, S. Qiu, *Chem. Rev.* **2017**, *117*, 1515 – 1156; d) F. Beuerle, B. Gole, *Angew. Chem. Int. Ed.* **2018**, *57*, 4850 – 4878; *Angew. Chem.* **2018**, *130*, 4942 – 4972; e) M. S. Lohse, T. Bein, *Adv. Funct. Mater.* **2018**, *28*, 1705553; f) Y. Song, Q. Sun, B. Aguila, S. Ma, *Adv. Sci.* **2019**, *6*, 1801410; g) H. Vardhan, A. M. Al-Enizi, A. Nafady, S. Ma, *Nanoscale* **2019**, *11*, 21679 – 21708.

[13] J. Jiang, Y. Zhao, O. M. Yaghi, *J. Am. Chem. Soc.* **2016**, *138*, 3255 – 3265.

[14] a) S. J. Lyle, P. J. Waller, O. M. Yaghi, *Trends Chem.* **2019**, *1*, 172 – 184; b) N. Huang, P. Wang, D. Jiang, *Nat. Rev. Mater.* **2016**, *1*, 16068; c) Y. Jin, Y. Hu, W. Zhang, *Nat. Rev. Chem.* **2017**, *1*, s41570.

[15] a) S.-L. Cai, K. Zhang, J.-B. Tan, S. Wang, S.-R. Zheng, J. Fan, Y. Yu, W.-G. Zhang, Y. Liu, *ACS Macro Lett.* **2016**, *5*, 1348 – 1352; b) Y. Zhu, S. Wan, Y. Jin, W. Zhang, *J. Am. Chem. Soc.* **2015**, *137*, 13772 – 13775; c) Y. Du, H. Yang, J. Whiteley, S. Wan, Y. Jin, S.-H. Lee, W. Zhang, *Angew. Chem. Int. Ed.* **2016**, *55*, 1737 – 1741; *Angew. Chem.* **2016**, *128*, 1769 – 1773; d) N. Huang, L. Zhai, D. E. Coupry, M. A. Addicoat, K. Okushita, K. Nishimura, T. Heine, D. Jiang, *Nat. Commun.* **2016**, *7*, 12325.

[16] a) S. Wan, F. Gándara, A. Asano, H. Furukawa, A. Saeki, S. K. Dey, L. Liao, M. W. Ambrogio, Y. Y. Botros, X. Duan, S. Seki, J. F. Stoddart, O. M. Yaghi, *Chem. Mater.* **2011**, *23*, 4094 – 4097; b) N. Keller, D. Bessinger, S. Reuter, M. Calik, L. Ascherl, F. C. Hanusch, F. Auras, T. Bein, *J. Am. Chem. Soc.* **2017**, *139*, 8194 – 8199; c) D. Bessinger, L. Ascherl, F. Auras, T. Bein, *J. Am. Chem. Soc.* **2017**, *139*, 12035 – 12042; d) D. D. Medina, T. Sick, T. Bein, *Adv. Energy Mater.* **2017**, *7*, 1700387.

[17] a) A. Nagai, X. Chen, X. Feng, X. Ding, Z. Guo, D. Jiang, *Angew. Chem. Int. Ed.* **2013**, *52*, 3770 – 3774; *Angew. Chem.* **2013**, *125*, 3858 – 3862; b) G. Lin, H. Ding, R. Chen, Z. Peng, B. Wang, C. Wang, *J. Am. Chem. Soc.* **2017**, *139*, 8705 – 8709; c) R. Chen, J.-L. Shi, Y. Ma, G. Lin, X. Lang, C. Wang, *Angew. Chem. Int. Ed.* **2019**, *58*, 6430 – 6434; *Angew. Chem.* **2019**, *131*, 6496 – 6500.

[18] X. Ding, J. Guo, X. Feng, Y. Honsho, J. Guo, S. Seki, P. Maitarad, A. Saeki, S. Nagase, D. Jiang, *Angew. Chem. Int. Ed.* **2011**, *50*, 1289 – 1293; *Angew. Chem.* **2011**, *123*, 1325 – 1329.

[19] S. Haldar, D. Chakraborty, B. Roy, G. Banappanavar, K. Rinku, D. Mullangi, P. Hazra, D. Kabra, R. Vaidhyanathan, *J. Am. Chem. Soc.* **2018**, *140*, 13367 – 13374.

[20] D. D. Medina, M. L. Petrus, A. N. Jumabekov, J. T. Margraf, S. Weinberger, J. M. Rotter, T. Clark, T. Bein, *ACS Nano* **2017**, *11*, 2706 – 2713.

[21] C. Montoro, D. Rodríguez-San-Miguel, E. Polo, R. Escudero-Cid, M. L. Ruiz-González, J. A. R. Navarro, P. Ocón, F. Zamora, *J. Am. Chem. Soc.* **2017**, *139*, 10079 – 10086.

[22] a) M. Calik, F. Auras, L. M. Salonen, K. Bader, I. Grill, M. Handloser, D. D. Medina, M. Dogru, F. Löbermann, D. Trauner, A. Hartschuh, T. Bein, *J. Am. Chem. Soc.* **2014**, *136*, 17802 – 17807; b) S. Jin, M. Supur, M. Addicoat, K. Furukawa, L. Chen, T. Nakamura, S. Fukuzumi, S. Irle, D. Jiang, *J. Am. Chem. Soc.* **2015**, *137*, 7817 – 7827; c) N. Keller, M. Calik, D. Sharapa, H. R. Soni, P. M. Zehetmaier, S. Rager, F. Auras, A. C. Jakowetz, A. Görling, T. Clark, T. Bein, *J. Am. Chem. Soc.* **2018**, *140*, 16544 – 16552; d) B. Gole, V. Stepanenko, S. Rager, M. Grgne, D. D. Medina, T. Bein, F. Wgrthner, F. Beuerle, *Angew. Chem. Int. Ed.* **2018**, *57*, 846 – 850; *Angew. Chem.* **2018**, *130*, 856 – 860; e) X. Chen, M. Addicoat, E. Jin, L. Zhai, H. Xu, N. Huang, Z. Guo, L. Liu, S. Irle, D. Jiang, *J. Am. Chem. Soc.* **2015**, *137*, 3241 – 3247.

[23] Y. Zhao, H. Liu, C. Wu, Z. Zhang, Q. Pan, F. Hu, R. Wang, P. Li, X. Huang, Z. Li, *Angew. Chem. Int. Ed.* **2019**, *58*, 5376 – 5381; *Angew. Chem.* **2019**, *131*, 5430 – 5435.

[24] J. Park, D. Feng, S. Yuan, H.-C. Zhou, *Angew. Chem. Int. Ed.* **2015**, *54*, 430 – 435; *Angew. Chem.* **2015**, *127*, 440 – 445.

[25] a) K. Lu, C. He, W. Lin, *J. Am. Chem. Soc.* **2014**, *136*, 16712 – 16715; b) M. Lismont, L. Dreesen, S. Wuttke, *Adv. Funct. Mater.* **2017**, *27*, 1606314.

Manuscript received: December 6, 2019
Accepted manuscript online: January 8, 2020
Version of record online: February 3, 2020

